One-pot solvothermal synthesis of $FePt/Fe_3O_4$ core–shell nanoparticles†

Chih-Wei Lai,[a] Yu-Hsiu Wang,[a] Borade Prajakta Uttam,[b] Yu-Chun Chen,[a] Jong-Kai Hsiao,*[bc] Chien-Liang Liu,[a] Hon-Man Liu,[b] Chun-Yen Chen*[d] and Pi-Tai Chou*[a]

Received (in Cambridge, UK) 27th June 2008, Accepted 15th August 2008
First published as an Advance Article on the web 19th September 2008
DOI: 10.1039/b810965f

***Via* a facile, one-pot solvothermal synthesis, highly uniform $FePt/Fe_3O_4$ core–shell nanoparticles are successfully developed, which further demonstrates their superiority in the MR imaging of living cells.**

In the field of magnetic resonance imaging (MRI)[1] superparamagnetic iron oxides (SPIOs) and ultra-small superparamagnetic iron oxides (USPIOs) have been ubiquitously used for enhancing contrast between normal and pathological tissues, as well as for indicating the status of organ function or blood flow.[2] Under an external magnetic field, SPIOs and USPIOs, within water surroundings, lead to a faster proton T_2 relaxation rate, and thus provide a good contrast image. With magnetic nanoparticles labelled by antibody or peptide, the capability of MRI to probe tumours, infections or infarctions has received much attention.[3–7] On the other hand, iron–platinum (FePt) nanoparticles, a material widely used in data storage and permanent magnetic nanocomposite, also possess a great potential in biomedicine. It was evaluated that the $FePt/CoS_2$ core–shell nanostructures have potential in anticancer nanomedicine.[8] One possible pharmacological mechanism lies in that the iron metal in FePt core is oxidized under acidic environment in the cell and the released Pt^{2+} ions may enter into the nucleus and/or mitochondria, inducing apoptosis through dsDNA binding. Other hybrid FePt bifunctional nanoparticles, such as FePt–CdS,[9] FePt–CdSe,[10] FePt–Au[11] and FePt–ZnS,[12] have recently been exploited owing to their dual optical and magnetic properties. However, the magnetization of FePt MNPs is generally too small (*e.g.*, $\sim$10 emu g^{-1} at 0.5 kOe applied field.) to be applied for the corresponding MRI research.[13]

Among Fe-domain bifunctional materials, the $FePt/Fe_3O_4$ core–shell nanostructure has attracted our avid attention. $FePt/Fe_3O_4$ nanoparticles are promising in media storage because FePt agglomerates can be avoided due to the protection of the Fe_3O_4 shell. According to our viewpoint, $FePt/Fe_3O_4$ MNPs may find ample biomedical applications, combining the latent Pt therapeutic unit and Fe_3O_4 MRI property. Herein, we report a facile, one-pot solvothermal synthesis of highly uniform $FePt/Fe_3O_4$ core–shell nanoparticles. Despite the power of solvothermal techniques in various syntheses of nanoparticles,[14,15] to our knowledge, none have been reported regarding the solvothermal approach to FePt and $FePt/Fe_3O_4$ magnetic nanoparticles (MNPs).

Previous synthesis of $FePt/Fe_3O_4$ MNPs was achieved *via* a two-step process, in which FePt nanoparticles prepared by the polyol process were taken as seeds, followed by addition of the iron precursor into the reaction solution for growth of iron oxide shell *via* a polyol process.[16] We also found that a high-pressure, high-temperature, solvothermal approach makes $FePt/Fe_3O_4$ nanoparticles synthesis much more facile. Moreover, the resulting $FePt/Fe_3O_4$ MNPs possess several unique properties such as significant enhancement of magnetization (*e.g.*, $\sim$60 emu g^{-1} at 0.5 kOe applied field), intact surface passivation and hence great dispersibility as well as the feasibility in transformation to water-soluble MNPs. After phase transfer, the water-soluble $FePt/Fe_3O_4$ MNPs were successfully applied in MRI as detailed below.

The concept of one-pot reaction lies in the fact that the spherical shape of Fe_3O_4 and FePt MNPs could be well controlled by hydrothermal and polyol processes.[17,18] Combining these two methods, we thus prepared FePt nanoparticles through mixing of iron pentacarbonyl, $Fe(CO)_5$, and platinum(II) acetylacetonate, $Pt(acac)_2$, precursors. $Pt(acac)_2$ was further reduced by hexadecane-1,2-diol.[19] Subsequently, solvent phenyl ether was added, followed by the injection of oleic acid and oleylamine (see ESI†). Here, $Pt(acac)_2$ was set to be the limiting reactant, and the molar ratio of $Fe(CO)_5$ *vs.* $Pt(acac)_2$ was 4 : 1. In our reaction system, it was found that reaction time also played a key role for improving the crystalline packing. Initially, the product of 1 h reaction time was centrifuged, re-precipitated from ethanol, and then analyzed. X-Ray diffraction (XRD) analysis (Fig. 1A) reveals (111) and (200) XRD peaks at 2θ = 40.9 and 47.6°, indicating the formation of face-centered cubic (fcc) FePt nanoparticles. *Via* solvothermal process, excess Fe-precursor, $Fe(CO)_5$, was then oxidized to form an iron oxide shell coating onto the FePt surface. After 6 h reaction time, the XRD patterns of the product show the characteristic reflections of 2θ values up to 35.5° (311) and 43.2° (400), which signify the presence of the ferrite phase Fe_3O_4 (Fig. 1B and C). Comparing Fig. 1A–C, the XRD peak of the ferric phase (311) reveals increasing peak intensity from 1 to 6 h of reaction time. The time-dependent results can be rationalized by the degree of Fe_3O_4 shell crystallization on the FePt surface. According to transmission electron microscopy (TEM) (see later), the

[a] *Department of Chemistry, National Taiwan University, Taipei, 106, Taiwan. E-mail: chop@ntu.edu.tw*
[b] *Department of Medical Imaging, National Taiwan University Hospital and College of Medicine, Taipei, Taiwan. E-mail: jongkai@gmail.com*
[c] *Institute of Biomedical Engineering, National Taiwan University, Taipei, 106, Taiwan*
[d] *Industrial Technology Research Institute-South, Nano powder & Thin Film Technology Center, Tainan, Taiwan. E-mail: cy_chen@itri.org.tw*

† Electronic supplementary information (ESI) available: Experimental section, including instrument information, and experimental procedure. See DOI: 10.1039/b810965f

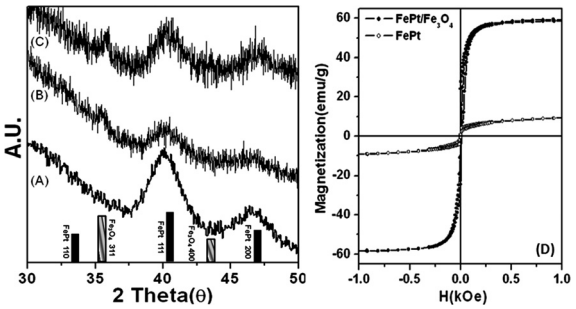

Fig. 1 XRD patterns of the MNPs after 1 h (A), 3 h (B) and 6 h (C) reaction time at 250 °C. (D) SQUID spectra of FePt and FePt/Fe_3O_4 MNPs at 300 K.

core–shell structure was formed after 3 h of reaction time, and no major structural change was observed upon extending this to 6 h. Magnetizations of FePt nanoparticles and FePt/Fe_3O_4 core–shell nanomaterial were measured immediately with a superconducting quantum interference device (SQUID) and found to be 11.2 and 59.5 emu g^{-1}, respectively, at 300 K. The shapes of the SQUID spectra confirmed their paramagnetic properties (Fig. 1D).

The uniform size of the as-prepared FePt and FePt/Fe_3O_4 is revealed in Fig. 2A and B, respectively. The average diameter was calculated to be 3.5 nm for FePt and 15.5 nm for FePt/Fe_3O_4. As the inset of Fig. 2A shows, the high-resolution TEM (HR-TEM) image indicates that FePt has a lattice spacing of 2.30 Å (111). Furthermore, the HR-TEM image of the FePt/Fe_3O_4 core–shell structure shown in Fig. 2C exhibits distinct crystalline structure of the FePt core and the Fe_3O_4 shell (see inset for the Fourier transform image of the electron diffraction pattern). The lattice spacing of the Fe_3O_4 shell was determined to be 2.97 Å (220). FePt/Fe_3O_4 nanoparticles were further analyzed by energy dispersive X-ray spectroscopy (EDX). The results shown in Fig. 2D unveil the elemental characteristic peaks of Cu (Kα: 8.040 eV, Lα: 0.930 eV, copper mesh), Fe (Kα: 6.403 eV, Lα: 0.705 eV) and Pt (Kα: 9.441 eV, Lα: 2.050 eV), rendering sufficient evidence for successful FePt/Fe_3O_4 formation.

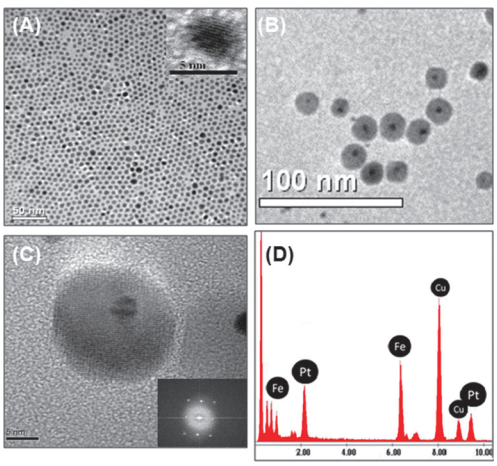

Fig. 2 (A) TEM images of samples with an average of 3.5 nm FePt MNPs (see inset) and (B) 15.5 nm FePt/Fe_3O_4 MNPs (scale bar = 100 nm). (C) the HRTEM image of FePt/Fe_3O_4 and its electron diffraction Fourier transform image (inset). (D) the EDX spectrum of FePt/Fe_3O_4.

Oleic acid/oleylamine coated FePt/Fe_3O_4 as prepared was water insoluble. To improve the bio-compatibility, subsequent ligand displacement was carried out. Knowing the relatively strong binding of oleic acid and oleylamine toward Fe_3O_4, seeking a suitable water-soluble ligand is crucial. As reported, 2,3-dimercaptosuccinic acid (DMSA) could be coated onto the Fe_3O_4 shell for phase transfer.[20] Accordingly, water-soluble FePt/Fe_3O_4 MNPs were prepared using a stepwise procedure reported by Chen *et al.*,[21] with slight modification. Detailed synthetic procedures are described in ESI.† Fig. 3A–C depict the infrared absorption spectra of DMSA water-soluble ligand, DMSA ligand-exchanged FePt/Fe_3O_4 MNP, and FePt/Fe_3O_4 MNP, respectively. The peaks at ~1550 cm^{-1} (see Fig. 3B and C) were assigned to the bidentate mode of –COO–M, while the shoulder peak at ~1630 cm^{-1} (denoted by *) represented the scissoring mode of molecularly bonded oleylamine. Compared to Fig. 3B, the ratio of peak intensity between the scissoring motion of amine (~1630 cm^{-1}) and the stretching motion of –COO–M (1550 cm^{-1}) in Fig. 3C is considerably reduced, indicating a partial removal of oleic acid after the phase transferring process.[22] Similar IR spectra have been reported, confirming that DMSA with carboxyl terminations coordinated to the iron atoms on the surface of MNPs.[23] As demonstrated in Fig. 3D, the FePt/Fe_3O_4/DMSA MNPs are water soluble as opposed to water-insoluble FePt/Fe_3O_4 prepared from the solvothermal reaction. The hydrodynamic radius of FePt/Fe_3O_4/DMSA after dissolving in water for more than one week was measured with dynamic light scattering (DLS). DLS data (see Fig. S1, ESI†) indicate uniform and well dispersed nanoparticles with a radius distribution of 25 ± 6 nm.

As for biological applications, human mesenchymal stem cell line (hMSCL) was adopted as a target (see ESI†). hMSCs was immortalized through over-expression of human telomerase reverse transcriptase (hTERT) with human papillomavirus E6 and E7.[24] The differentiation ability of these hMSCs has been extensively demonstrated.[25] After overnight incubation with 25 μg mL^{-1} FePt/Fe_3O_4/DMSA MNPs, microscopic imaging study of living hMSCs was carried out with an inverted microscope (Nikon ECLIPSE TE 2000-U). As shown in Fig. 4A and B, an appreciable amount of granules spread

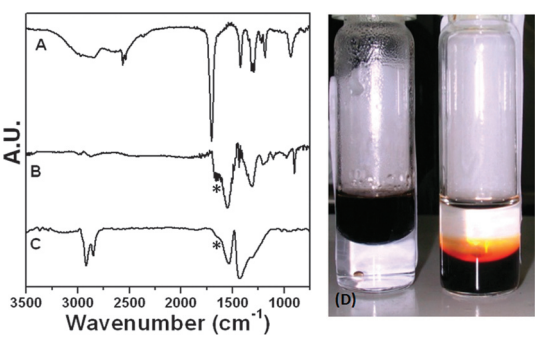

Fig. 3 (A) FTIR spectra of water–soluble ligand DMSA, (B) FePt/Fe_3O_4 MNP–DMSA complex and (C) as-prepared FePt/Fe_3O_4 MNP with the peaks of bidentate (–COO–M) at ~1550 cm^{-1}. (D) Left cuvette (upper phase: toluene, lower phase: water) unmodified FePt/Fe_3O_4 in toluene phase. Right cuvette: DMSA modified FePt/Fe_3O_4 in water phase.

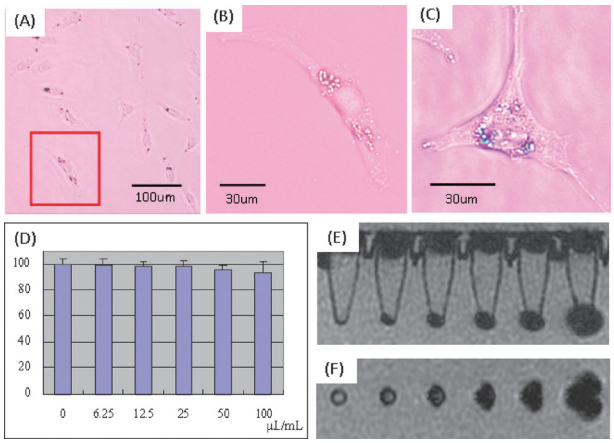

Fig. 4 (A) 20× bright field image of living hMSCs after overnight incubation with 25 μg mL^{-1} $FePt/Fe_3O_4$ MNPs, and (B) a 40× regional magnification of (A) as indicated in the red block. (C) 40× bright field image of hMSCs with Prussian blue stain. (D) Cell viability test results of hMSCs after 48 h incubation with $FePt/Fe_3O_4$ nanoparticles with serial concentrations. (E) and (F) are MR images of hMSC pellets with different view angles, using the same dosage as applied in cell viability tests. Cell numbers in different microcentrifuges were well controlled (1×10^4 cells/microcentrifuge).

around cell nucleus was observed. To confirm if these granules were $FePt/Fe_3O_4$/DMSA MNPs, Prussian blue stain was used for Fe^{3+} staining to further identify these granule-like structures. Prussian Blue staining agent was freshly prepared by mixing 1 M HCl aqueous solution with 2% ferrocyanide in 1 : 1 ratio. When cell samples were treated with acid solutions of ferrocyanides, ferric ion(III) in cell samples would combine with ferrocyanide and result in formation of the bright blue ferric ferrocyanide pigment, as shown in Fig. 4C. The results further identified that these granules were taken up from $FePt/Fe_3O_4$/DMSA MNPs.

For cytotoxicity tests, different amount of particles were added to each hMSC sample to reach final concentrations of 0, 6.25, 12.5, 25, 50 and 100 μg mL^{-1}. The result from the MTT (3-(4,5-dimethylthiazol-2-yl)-2,5-diphenyltetrazolium bromide) test, as shown in Fig. 4D, reveals almost 95% cell viability is achieved after cells were incubated with 100 μg mL^{-1} of $FePt/Fe_3O_4$/DMSA MNPs even for 48 h (see ESI† for details)

In MRI study, six cell samples were respectively pre-treated with 0, 6.25, 12.5, 25, 50 and 100 μg mL^{-1} of $FePt/Fe_3O_4$/DMSA MNPs for 24 h, where 1×10^4 cells/microcentrifuge was used. Cell samples were then harvested through trypsinization and collected as cell pellets in 200 μL microcentrifuges for imaging study. Different view angles of MR images of collected cell pellets are shown in Fig. 4E and F. The significant dosage response in MRI study and its low cytotoxicity in viability test both proved that these particles could be applied for specific bio-targeting or *in vivo* MR imaging. The quantification of cellular uptake was further performed by measuring the optical density of $FePt/Fe_3O_4$/DMSA MNPs treated cells at 247.3 nm using a UV/Visible spectrophotometer. As a result, a rising exponential-like plot for particle uptake *vs.* pre-added $FePt/Fe_3O_4$/DMSA was obtained (see Fig. S2 in ESI†), the result of which qualitatively correlates with the dose dependent behavior observed in MRI study.

In conclusion, the present work reveals several interesting features concerning $FePt/Fe_3O_4$ MNPs. First is through one-pot, solvothermal reaction, a facile synthesis of $FePt/Fe_3O_4$ core–shell MNPs is achieved. The resulting MNPs possess high uniformity of FePt (~3.5 nm, core) and consequent $FePt/Fe_3O_4$ core–shell nanoparticles of ~15.5 nm. And second, the $FePt/Fe_3O_4$ MNPs are easily modified and transformed to water-soluble $FePt/Fe_3O_4$/DMSA MNPs, which then demonstrated their superiority in the MR image of living cells. The iron metal of this nanocomposite might further be oxidized under *e.g.* acidic environment, releasing Pt^{2+} ions and therefore inducing cell apoptosis. Due to the homogeneity and facile synthetic route, the one-pot, solvothermal synthesis of $FePt/Fe_3O_4$ MNPs should find importance in bio-imaging and chemical therapy.

Notes and references

1 A.-H. Lu, E. L. Salabas and F. Schűth, *Angew. Chem., Int. Ed.*, 2007, **46**, 1222.
2 W. S. Enochs, G. Harsh, F. Hochberg and R. Weissleder, *J. Magn. Reson. Imaging*, 1999, **9**, 228.
3 D. Hogemann, V. Ntziachristos, L. Josephson and R. Weissleder, *Bioconjugate Chem.*, 2002, **13**, 116.
4 N. Nitin, L. E. W. LaConte, O. Zurkiya, X. Hu and G. Bao, *J. Biol. Inorg. Chem.*, 2004, **9**, 706.
5 J.-S. Choi, H. J. Choi, D. C. Jung, J.-H. Lee and J. W. Cheon, *Chem. Commun.*, 2008, 2197.
6 C. Bárcena, A. K. Sra, G. S. Chaubey, C. Khemtong, J. P. Liu and J. M. Gao, *Chem. Commun.*, 2008, 2224.
7 J. Wan, W. Cai, X. G. Meng and E. Z. Liu, *Chem. Commun.*, 2007, 5004.
8 J. Gao, G. Liang, B. Zhang, Y. Kuang, X. Zhang and B. Xu, *J. Am. Chem. Soc.*, 2007, **129**, 1428.
9 H. Gu, R. Zheng, X. Zhang and B. Xu, *J. Am. Chem. Soc.*, 2004, **126**, 5664.
10 J. Gao, B. Zhang, Y. Gao, Y. Pan, X. Zhang and B. Xu, *J. Am. Chem. Soc.*, 2007, **129**, 11928.
11 J. S. Choi, Y. W. Jun, S. I. Yeon, H. C. Kim, J. S. Shin and J. Cheon, *J. Am. Chem. Soc.*, 2006, **128**, 15982.
12 H. Gu, R. Zheng, H. Liu, X. Zhang and B. Xu, *Small*, 2005, **1**, 402.
13 S. Sun, *Adv. Mater.*, 2006, **18**, 393.
14 N. Bao, L. Shen, Y. Wang, P. Padhan and A. Gupta, *J. Am. Chem. Soc.*, 2007, **129**, 12374.
15 C.-W. Lai, Y.-H. Wang, C.-H. Lai, M.-J. Yang, C.-Y. Chen, P.-T. Chou, C.-S. Chan, Y. Chi, Y.-C. Chen and J.-K. Hsiao, *Small*, 2008, **4**, 218.
16 H. Zeng, J. Li, Z. L. Wang, J. P. Liu and S. H. Sun, *Nano Lett.*, 2004, **4**, 187.
17 S. Sun and H. Zeng, *J. Am. Chem. Soc.*, 2002, **124**, 8204.
18 H. Deng, X. Li, Q. Peng, X. Wang, J. Chen and Y. Li, *Angew. Chem., Int. Ed.*, 2005, **44**, 2782.
19 S. Sun, C. B. Murray, D. Weller, L. Folks and A. Moser, *Science*, 2000, **287**, 1989.
20 M. Kim, B. Lim, Y. Jeong, Y. Cho and Y. Choa, *J. Ceram. Process. Res.*, 2007, **8**, 293.
21 C.-Y. Chen, C.-T. Cheng, C.-W. Lai, P.-W. Wu, K.-C. Wu, P.-T. Chou, Y.-H. Chou and H.-T. Chiu, *Chem. Commun.*, 2006, 263.
22 N. Shukla, C. Liu, P. M Jones and D. Weller, *J. Magn. Magn. Mater.*, 2003, **266**, 178.
23 H. G. Bagaria, E. T. Ada, M. Shamsuzzoha, D. E. Nikles and D. T. Johnson, *Langmuir*, 2006, **22**, 7732.
24 T. Okamoto, T. Aoyama, T. Nakayama, T. Nakamata, T. Hosaka, K. Nishijo, T. Nakamura, T. Kiyono and J. Toguchida, *Biochem. Biophys. Res. Commun.*, 2002, **295**, 354.
25 J.-K. Hsiao, M.-F. Tai, H.-H. Chu, S.-T. Chen, H. Li, D.-M. Lai, S.-T. Hsieh, J.-L. Wang and H.-M. Liu, *Magn. Reson. Med.*, 2007, **58**, 717.